Check for updates

A Fully Integrated Miniaturized Optical Biosensor for Fast and Multiplexing Plasmonic Detection of High- and Low-Molecular-Weight Analytes

Margherita Bolognesi,* Mario Prosa, Michael Toerker, Laura Lopez Sanchez, Martin Wieczorek, Caterina Giacomelli, Emilia Benvenuti, Paola Pellacani, Alexander Elferink, Andreas Morschhauser, Laura Sola, Francesco Damin, Marcella Chiari, Mark Whatton, Etienne Haenni, David Kallweit, Franco Marabelli, Jeroen Peters, and Stefano Toffanin*

Optical biosensors based on plasmonic sensing schemes combine high sensitivity and selectivity with label-free detection. However, the use of bulky optical components is still hampering the possibility of obtaining miniaturized systems required for analysis in real settings. Here, a fully miniaturized optical biosensor prototype based on plasmonic detection is demonstrated, which enables fast and multiplex sensing of analytes with high- and low molecular weight (80 000 and 582 Da) as quality and safety parameters for milk: a protein (lactoferrin) and an antibiotic (streptomycin). The optical sensor is based on the smart integration of: i) miniaturized organic optoelectronic devices used as light-emitting and light-sensing elements and ii) a functionalized nanostructured plasmonic grating for highly sensitive and specific localized surface plasmon resonance (SPR) detection. The sensor provides quantitative and linear response reaching a limit of detection of 10^{-4} refractive index units once it is calibrated by standard solutions. Analyte-specific and rapid (15 min long) immunoassay-based detection is demonstrated for both targets. By using a custom algorithm based on principal-component analysis, a linear dose–response curve is constructed which correlates with a limit of detection (LOD) as low as 3.7 µg mL^{-1} for lactoferrin, thus assessing that the miniaturized optical biosensor is well-aligned with the chosen reference benchtop SPR method.

1. Introduction

In recent years, ever-increasing effort has been devoted to the research and development of new sensing technologies for fast, accurate, and low-cost analytical detection of relevant targets for environmental monitoring, healthcare or food safety and quality. Other than focusing on improved performance, one of the main challenges in these sensing technologies is their transfer out of the laboratory into real-setting scenarios such as point-of-need (PON) or point-of-care (POC) systems.[1]

The majority of POC systems already present on the market are lateral flow devices, such as pregnancy or COVID-19 rapid tests, or electrochemical sensing-based glucometers.[2–3] However, their sensing capability is quite limited, being either only qualitative or restricted to the detection of a single analyte. The potential of POC and PON systems is now focused on performing more complex analysis, such as highly sensitive, specific, quantitative and

M. Bolognesi, M. Prosa, E. Benvenuti, S. Toffanin
Institute of Nanostructured Materials (ISMN) – National Research Council (CNR)
Via P. Gobetti 101, Bologna 40129, Italy
E-mail: margherita.bolognesi@cnr.it; stefano.toffanin@cnr.it

M. Toerker, M. Wieczorek
Fraunhofer FEP
Winterbergstraße 28, 01277 Dresden, Germany

L. Lopez Sanchez, P. Pellacani
Plasmore s.r.l
Viale Vittorio Emanuele II 4, Pavia 27100, Italy

C. Giacomelli
KODE s.r.l.
Lungarno Galileo Galilei 1, Pisa 56100, Italy

A. Elferink, J. Peters
Wageningen Food Safety Research – Wageningen University and Research
Akkermaalsbos 2, Wageningen 6708 WB, The Netherlands

A. Morschhauser
Fraunhofer ENAS
Technologie – Campus 3, 09126 Chemnitz, Germany

**ADVANCED
SCIENCE NEWS**

www.advancedsciencenews.com

**ADVANCED
MATERIALS**

www.advmat.de

label-free detection of multiple analytes, with simple sample preparation, still in a fast and accurate way. Besides the requirement of high sensitivity and specificity, an appropriate miniaturized biosensor should also be capable of integration, automation and multiplex detection for use in areas where well-trained personnel may not be available and in-line/at-line rapid measurements are needed. Although many studies have reported the integration of miniaturized biosensors, it remains challenging to develop a fully integrated device in a robust, and user-friendly format.[4] The smart integration of multiple miniaturized and advanced technological components that are related to micro/nanoelectronics,[5–6] nanophotonics,[7] microfluidics,[8–9] and functionalized transducing surface is required.[10]

In this context refractive-index-based (or refractometric) sensing systems have a great potential thanks to not only their high sensitivity, ease of use, rapid response and low cost, but also the possibility to perform label-free detection.[11] However, the process of miniaturization is still immature due to technical problems for miniaturized optical-related instrument parts, such as illumination systems and spectrometers,[12–13] and only recently refractometric sensors are being developed for both miniaturization and multiplexed detection.[14] By considering surface-plasmon resonance (SPR) refractomeric sensors, the use of the typical prism- or grating-based Kretschmann backscattering geometry allows to perform measurements also in turbid samples (such as blood, milk, ...), differently from other detection schemes.[11]

Organic optoelectronic devices are demonstrating significant benefits for PON and POC systems,[15] not only for their ever-improving optical performance[16–21] but also for the inherent feature of being miniaturized in sensor architectures.[6] In our recent work we realized an optics-less and prism-free, grating-based intensity modulated SPR sensor, with a total chip volume as low as 0.1 cm^3 based on organic optoelectronic devices.[22] Such a high level of miniaturization was possible by the monolithic integration and device stack on a single substrate of coplanar organic light sources and light detectors, with optimally matched spectral characteristics and geometry, along with the implementation of a nanoplasmonic grating (NPG) directly onto the thin encapsulating glass of the optoelectronic components.

The NPG is composed of an hexagonal arrangement of nanoholes filled with polymeric pillars onto a gold surface: this specific design of the NPG is responsible for supporting a combination of both SPR and localized SPR (LSPR) modes on its sur-face, that shift their spectral response when exposed to a refractive index change of the surrounding medium.[23–24]

In this work, we further proceed in the realization of a field-applicable PON system by implementing an immunoassay-based biorecognition system for selective and sensitive multiplexed biosensing onto the NPG surface once coupled to the miniaturized organic optoelectronic system.[25–26] To note, the NPG is favorable to biofunctionalization thanks to its chemical composition and smooth surface morphology.[23] Given their easy target engineering, specificity and great affinity toward a variety of biological analytes,[27] different immunoassay-based biorecognition elements are used for functionalizing different regions (i.e., channels) of the NPG surface (and thus the active surface of the SPR biosensor itself).[24] This enables: i) label-free detection of multiple analytes in a 15 min single sample measurement and ii) easy washing procedure for regenerating the functioning of the surface for multiple measurements.

The final step in the realization of the stand-alone and functional prototype of the SPR biosensor is the integration of a microfluidic module and an ad hoc electronics and hardware for amplification and fast read-out. The broad applicability of the as-designed sensor for multiplexing in real settings is demonstrated by selecting two model high- and low-molecular-weight targets within the quality and safety parameters in the milk chain: lactoferrin (a protein), and streptomycin (an antibiotic). Lactoferrin is a quality factor of milk,[28] as well as an important animal-safety biomarker in cow's milk, i.e., for detecting mastitis, a bacterial inflammation of the udders.[29] Lactoferrin is a high-molecular-weight target (80 000 Da), thus a direct immunoassay-based method is typically used for SPR-based detection,[30–31] as in the present work. Streptomycin is a low-molecular-weight target (582 Da) which belongs to the group of the aminoglycoside antibiotics. Its use in farm animals and the eventual transfer to meat, milk, and other dairy products,[32] can lead to the well-publicized problem of antimicrobial resistance and consequent wide-ranging threat to human health.[33] For the detection of streptomycin, a competitive immunoassay is implemented since this approach is the most effective in measuring small analytes through SPR.[34]

Finally, the collected sensorgrams both related to the self-testing procedure with standard solutions and detection of targets analytes in buffer solutions are statistically analyzed by means of a custom algorithm based on principal-component analysis in order to determine the limit of detection (LOD) of the proposed assays in the SPR biosensor prototype, in terms of refractive-index units and lactoferrin concentration. These results are comparable to a reference benchtop SPR analytical instrument, namely BIACORE 3000.

2. Results and Discussion

2.1. Design and Fabrication of the Optoplasmonic Chip

The SPR biosensor prototype is formed of several components, which have been designed, fabricated and sequentially assembled (following the steps schematized in Figure S1 in the Supporting Information) to perform different functions.

The core of the SPR biosensor prototype is the optoplasmonic chip sketched in **Figure 1**a. The layout and interaction

L. Sola, F. Damin, M. Chiari
SCITEC Istituto di Scienze e Tecnologie Chimiche "G. Natta" – National Research Council (CNR)
Via Mario Bianco 9, Milano 20131, Italy

M. Whatton
QuadraChem Laboratories Ltd (QCL)
Riverside – Forest Row Business Park, East Sussex RH18 5DW, UK

E. Haenni, D. Kallweit
CSEM Center Muttenz
Tramstrasse 99, Muttenz CH-4132, Switzerland

F. Marabelli
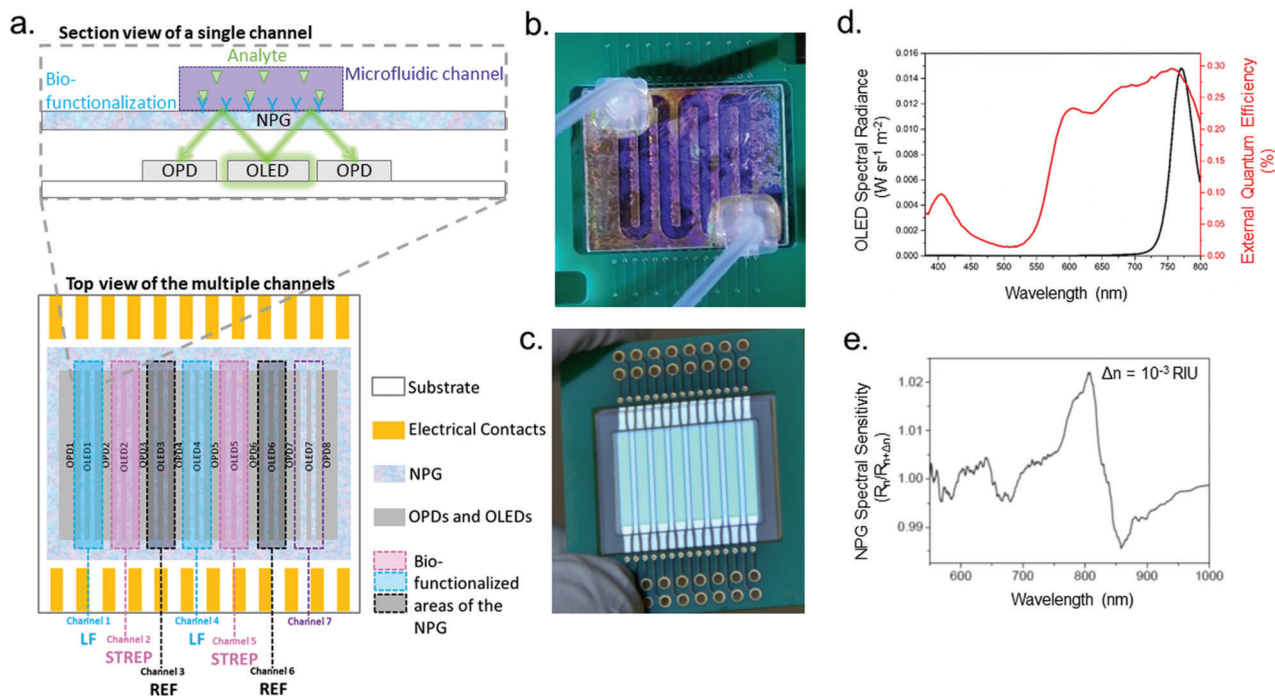Physics Department – University of Pavia
Via A. Bassi 6, Pavia 27100, Italy

2208719 (2 of 13)

Figure 1. a) Schematic representation of the sensor chip, working in backscattering configuration with intensity-modulated SPR detection. The top panel shows a section view of a single channel comprising an organic light emitting diode (OLED) and two organic photodiodes (OPDs) monolithically integrated onto the same substrate and a nanoplasmonic grating (NPG) functionalized on the top side with biorecognition elements, for the selective immobilization of the target analyte(s) transported on the sensing surface by the microfluidic circuitry. The bottom panel shows a top view of the sensor chip comprising multiple channels for the parallel detection of multiple analytes. The multichannel optoplasmonic sensor chip is composed of 8 OPDs and 7 OLEDs, aligned under the 7 areas of the NPG covered with the analyte-specific biofunctionalization; each channel is defined by the area of the surface where biofunctionalization toward lactoferrin (LF) or streptomycin (STREP) is present, or where there is no biofunctionalization (reference, REF); the signal from a channel is acquired by switching on the OLED in the center of the channel and acquiring the photocurrent from one of the two adjacent OPDs. b) Picture from the top view of the optoplasmonic chip with the meander microfluidic flow cell attached on top of the NPG, covering the 7 channels of the sensor chip. c) Photograph of a sensor chip encapsulated with a transparent cap with no NPG on top, to allow viewing the multiple OLEDs and OPDs schematized in (a). d) Spectral radiance of a reference OLED driven at 31.69 mA cm^{-2} and external quantum efficiency of the OPD. e) Spectral sensitivity of the NPG for a refractive index change (Δn) of $\approx 10^{-3}$ RIU (refractive index units) at the NPG surface, calculated as the ratio of the reflectivity spectra with the NPG exposed to a 1% sucrose solution and water, measured at normal incidence.

between optoelectronic and plasmonic components in a single channel of the optoplasmonic chip are reported in the section view in the top panel of Figure 1a. Detection is based on SPR in a grating-coupled Kretschmann backscattering configuration and exploits miniaturized light-emitting and light-sensing components, that are organic light-emitting diodes (OLEDs) and organic photodiodes (OPDs) respectively, and a biofunctionalized nanoplasmonic grating (NPG) as the sensing surface. SPR sensors are typically classified into angular-, wavelength-, or intensity-modulated systems. Our system is based on intensity-modulation: the excitation light from the OLED, impinging on the NPG sensing surface at fixed angle(s) and wavelength(s), is intensity-modulated according to the variation of refractive index at the grating, and backscattered. The three elements are integrated to detect the refractive index variation upon analyte recognition at the NPG sensing surface, and to convert the intensity modulation in an electrical output. Specifically, light emitted by the OLED impinges the backside of the NPG, whose reflectivity is modulated upon the capture of analytes by the bioreceptors anchored at its topside. The ratio between the modulated signal and the base unmodulated signal, collected and transduced by the OPD, is the final signal from the sensor. We highlight that

our SPR sensor is different from typical intensity-modulation SPR sensors and instruments since: i) no optic system is used for coupling the impinging light with the plasmons of the sensing surface and ii) OLEDs implemented as light sources are not collimated and monochromatic, differently from the typical light sources (LEDs, lasers) used in intensity-modulation SPR sensors. Therefore, a broad range of incidence/collecting angles and excitation wavelengths (distributed according to the electroluminescence spectrum and angular emission profile of the OLED, respectively) all favorably contribute to the intensity-modulated signal collected and transduced by the OPD.

For the design of the optoplasmonic chip layout, simulations were carried out with proprietary software developed in our previous work.[22] The optimization of the geometry of the integrated system under consideration is particularly challenging due to the multiple wavelengths and multiple angles contributing to the final SPR signal from the sensor. Optical simulations were implemented and optimized to fit all geometrical and optical parameters of the photonic and plasmonic components (Experimental Section and Figure S2 in the Supporting Information). According to our prior work,[22] simulations on a similar system indicated that the lateral distance between the light source and the light

2208719 (3 of 13)

ADVANCED
SCIENCE NEWS
www.advancedsciencenews.com

ADVANCED
MATERIALS
www.advmat.de

detector is the parameter to optimize in order to favor the collection of photons once they are reflected by the NPG at quasi-normal incidence (i.e., small angles), which is the geometrical condition that guarantees the largest SPR modulation. In addition, the lateral distance between adjacent OLEDs and OPDs must also fulfill fabrication requirements and accuracies. Finally, interchannel crosstalk should be minimized. Therefore OLEDs were fabricated as light emitting independent stripes, side-by-side and alternating with the OPD light-sensing stripes, at an edge-to-edge distance of 320 µm (Figure S3, Supporting Information). The final optoplasmonic chip layout is also designed to maximize the lateral size of the multiple OLED and OPD stripes fabricated onto the same substrate, as a trade-off between i) a high number of active channels onto the same substrate, to allow sensing of multiple analytes onto the same chip, and ii) large active areas of the OPDs and OLEDs to maximize the signal collected by the electronic hardware.

The final optoplasmonic chip includes 7 different channels (scheme in Figure 1a and picture in Figure 1c): each channel includes one OLED for light excitation, two independent OPDs for light collection and signal transduction (one OPD on each side of the OLED), a target-selective biofunctionalization region on the NPG. Thus, each single channel is sensitive and selective toward a specific analyte. In this work, two channels are selective toward lactoferrin, two toward streptomycin and two are used as signal reference, while one channel was not used (bottom panel of Figure 1a). The meander microfluidic cell (picture in Figure 1b) covers all the 7 channels of the sensor chip and conveys the reference solutions, or the solution to be analyzed, on all channels. Therefore multiple analytes can be measured at the same time in different channels onto the same chip, thanks to the different biofunctionalization in the different regions of NPG and to the independent switching of OLEDs relating to the different channels.

Spectral matching between the optoelectronic and plasmonic components of the chip is achieved by designing ad hoc the single components. The OLED includes the emitting solid state blend of Pt^{II}-tetraphenyltetrabenzoporphyrin and tris(8-hydroxyquinoline) aluminum, which shows an electroluminescence spectrum with a narrow peak centered at 760 nm (Figure 1d). This emissive layer is embedded in a stack architecture composed of charge selective interlayers, a bottom Ag electrode and a semitransparent Ca/Ag top electrode covered by an index matching layer, for an efficient extraction of the emitted light out of the device stack. The optical power of the OLEDs increases when the operating current increases, although at the expense of efficiency (Figure S4, Supporting Information). An acceptable trade-off is found when operating the OLED at a current of around 1.1 mA (current density of 10 mA cm^{-2}), which yields an optical power of around 30 µW (optical power density of 0.3 mW cm^{-2} considering the emitting area).

The OPD is based on a blend of zinc phthalocyanine and fullerene-C60 light-absorbing layer. The thickness of all layers was optimized for maximum sensitivity in the near-infrared (NIR) region. The external quantum efficiency (EQE) of the OPD (Figure 1d) is peaked at 755 nm with a value of 30%, and almost perfectly matches the emission peak of the OLED and a relative maximum sensitivity of the NPG for low refractive index variations, at a quasi-normal incident angle. In addition, the OPD op-

erated at zero bias conditions (i.e., in short circuit) shows a linear photocurrent response under illumination with an external light source peaked at 770 nm, in the range of the optical power of the OLED in the defined working conditions (1–30 µW, Figure S5, Supporting Information).

The optimized and matched spectral, optical, and geometrical features of the single photonic components must also match those of the NPG. The NPG is a hexagonal lattice of polymeric pillars embedded in a thin gold film. A scanning electron microscopy (SEM) image of the NPG and a schematic representation of its lattice dimensions are reported in Figure S6 (Supporting Information). The NPG is prepared by colloidal lithography and plasma etching techniques as reported in our previous work.[22] The emission spectrum from the OLED and the spectral response of the OPD (i.e., EQE) both perfectly overlap with the maximum sensitivity of the NPG at quasi-zero angle of incidence. Specifically, the sensitivity of the NPG is defined as the ratio between reflectance spectra measured at quasi-normal incidence, when exposing the NPG surface to two liquids with different refractive indexes. Here, a bulk refractive index change (Δn) of 10^{-3} refractive index units (RIU) at the NPG surface was tested by exposing the NPG to a sucrose solution at 1% volume concentration, and to ultrapure water. To note, a Δn of $\approx 10^{-3}$ RIU roughly corresponds to the refractive index change given by a solution containing 50 µg mL^{-1} of lactoferrin, as measured by the benchtop SPR instrument from Biacore. For this Δn, the maximum sensitivity of the NPG, in the vis-NIR spectral range, is peaked at 770 nm, perfectly matching the OLED emission maximum, with a value of 2% (Figure 1e).

2.2. Assay Development on SPR Benchmark Instrument

For the implementation of biorecognition elements at the NPG surface of the sensor, assays were previously developed on a benchtop SPR instrument from Biacore. Specifically, a direct capture immunoassay for lactoferrin by lactoferrin polyclonal antibody (pAb) and an indirect competitive immunoassay for the detection of streptomycin (by a streptomycin–protein conjugate, strep-BSA, and streptomycin monoclonal antibody, strep-mAb) were developed. The schematic principles of operation can be found in Figures S7 and Figure S8 (Supporting Information) respectively.

From the injected lactoferrin standard solutions, a satisfactory dose–response curve can be constructed (**Figure 2**a) using a nonlinear fit model. With this constructed dose–response curve, the range of natural occurrence of lactoferrin in milk samples can be assessed (tens to hundreds of µg mL^{-1}). For higher concentrations of lactoferrin, that normally occur during bacterial udder infection (>300 µg mL^{-1}), samples may need to be diluted for determining the exact concentration of lactoferrin. The injection of a commercial skimmed milk sample resulted in a lactoferrin concentration of 75 µg mL^{-1} based on the dose-response curve shown in Figure 2a.

Similarly, the sensitivity of the developed streptomycin assay was tested by injection of a range of streptomycin standard solutions, each mixed with the same amount of streptomycin mAb. From these injections a dose–response curve was constructed, using 5 parameter logistics. Based on this curve (Figure 2b),
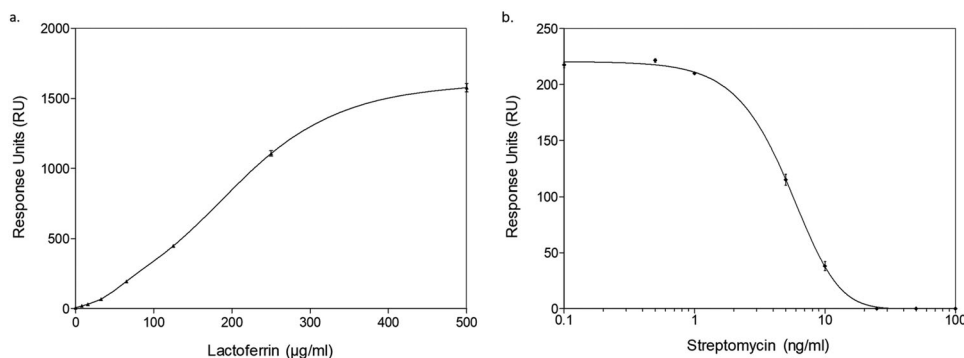
**ADVANCED
SCIENCE NEWS**

www.advancedsciencenews.com

**ADVANCED
MATERIALS**

www.advmat.de

Figure 2. a,b) Dose–response curves for lactoferrin (a) and streptomycin (b) assays as measured in the benchmark SPR instrument Biacore.

detection of streptomycin at the maximum residue level (MRL) set by law, that is 200 ng mL^{-1}, is easily feasible. The sensitivity of the assay even allows a 10- to 40-fold dilution of a milk samples to stay in the desired MRL-based detection range. The streptomycin mAb used for the development of the assay was able to detect both streptomycin and di-hydrostreptomycin. Cross-reactivity testing for the aminoglycosides group showed no response to apramycin, gentamycin, tobramycin, neomycin, paromycin, spectinomycin and kanamycin, not even in very high concentrations (1 µg mL^{-1}).

2.3. Biofunctionalization at the Sensing Surface

An important step inherent to the realization of sensing surfaces in biosensors and their implementation for high-throughput tests is to conceive a functional coating that: 1) provides a desired concentration of receptors; 2) preserves their biological activity; and 3) suppresses the nonspecific adsorption of nontarget molecules. For points (1) and (2), in this study we used the commercial co-polymer MCP-2F as functional coating of the NPG surface. The MCP-2F copolymer interacts strongly with several materials through a variety of mechanisms including hydrophobic interactions, van der Waals forces and hydrogen bonds.[35] This makes this polymer appropriate for the coating of the heterogeneous surface of the NPG. The NAS unit from the polymer exhibits the *N*-hydroxysuccinimide group that allows the covalent binding of any biomolecule containing primary amine groups, including the selected bioreceptors. For point (3), the remaining parts of the chip that were not biofunctionalized were passivated by using a commercial blocking buffer capable of suppressing nonspecific adsorption of nontarget molecules (see the Experimental Section).

Immobilization of the proteins following this protocol was corroborated by fluorescence measurements carried on functionalized NPGs (Figure S9, Supporting Information). Activity and stability of the interaction with the counterparts of the immobilized proteins were demonstrated through measurements of biofunctionalized sensor surfaces in iSPR (data not shown).

2.4. Assembly and Assessment of the SPR Biosensor Prototype

The developed optoplasmonic chip and assays were combined and tested in the complete SPR biosensor prototype. To allow

the detection of the low photocurrent signals from the optoplasmonic chip, a stand-alone electronic hardware, which includes low noise, accurate, fast response and miniaturized electronic components, was developed (see description in the Experimental Section). As estimated from simulations (Experimental Section and Figure S2, Supporting Information), the expected signal from each OPD of each sensing channel, for a $\Delta n \approx 10^{-3}$ RIU at the NPG surface, is about a 300 pA of photocurrent variation over a base photocurrent of 0.1 µA (0.3% signal variation). The fabricated electronic hardware demonstrated a resolution and accuracy far below the ones required for the signal expected from simulations.

Also, all the microfluidic circuitry elements were developed ad hoc, together with precise alignment procedures on the optoplasmonic chip, as described in the Experimental Section, to be employed in the complete SPR biosensor prototype. This design allowed the biofunctionalized surface area of the NPG to be exposed to a constant flow of the reference solutions and to analytes. An automatic syringe pump was connected to the meander microfluidic circuitry allowing for a controlled and constant liquid volume and flux during the immunoassays. This scheme resulted in reliable analytical assays with a limited sample volume (tens to hundreds of microliters) in a short time (up to 15 min), with a good repeatability between all the measurements (self-testing and calibration).

The experimental data from the self-testing measurements described in the following section (see Figure S10 in the Supporting Information for an example of raw output data) with the complete SPR biosensor prototype resulted in a 20-fold larger base photocurrent (i.e., around 2 µA) and a 3-fold lower signal variation (i.e., a few nA, that is around 0.1% of signal variation) compared to simulations, for the same $\Delta n \approx 10^{-3}$ RIU. This discrepancy could be easily explained by considering the dataset used for the simulations: i) reflectivity of the NPG at the small angles was possibly underestimated; ii) spectral data beyond 800 nm were neglected although seeming to include a significant part of the optical power of the OLED and of the spectral response of the OPD. However, despite these discrepancies, the developed electronic hardware had a resolution and accuracy higher than the one required for reading the signal at the LOD (around 200 pA, see below and Section 2.5.2).

To provide reliability and reproducibility in the results when the SPR biosensor prototype is used for quantitative measurements of the analytes of interest, a self-testing procedure was

**ADVANCED
SCIENCE NEWS**

www.advancedsciencenews.com

**ADVANCED
MATERIALS**

www.advmat.de

developed. The procedure consists of measuring the response of the SPR biosensor prototype to known refractive-index changes (Δn) at the NPG surface, by collecting the OPD output photocurrent over time when the OLED is in the ON state and the NPG surface is alternatively exposed to reference sucrose solutions and ultrapure water.

Aqueous sucrose solutions at variable volume concentrations (from 5% to 0.1%) were tested, covering a range of Δn of more than two orders of magnitude (Δn from $\approx 10^{-2}$ to $\approx 10^{-4}$ RIU), in the expected range of Δn occurring in the quantitative assays (i.e., concentration of lactoferrin in milk of lactating cows).[29] The outputs of the self-testing procedure are: i) to control and confirm the linearity of the dose-response curve in all sensing channels/for all OPDs; ii) the definition of the correction factor of the OPDs, for the quantification of the response of each OPD of each channel to the same Δn occurring at the sensing surface. In Figure S11 we report a scheme of the typical profile obtained by using SPR-based methods for measuring refractive-index variations in liquids where the reference and measure signals are reported. The channel-specific correction factor is extrapolated to be used for the quantitative assay analysis (see infra).

Given the multistep procedures of the self-testing and of the measure of the biological targets, and to avoid any user-dependency on data elaboration and enable the operability of the sensor even by nonexperts, data analysis through principal components analysis (PCA) was performed on the raw data (see Statistical Data Analysis in the Experimental Section).[36] PCA can be used to reduce the dimensionality of a dataset through a linear transformation of the data in a new coordinate system, in which most of their variation can be described with smaller dimensions than the initial ones. In details, the novel algorithm that we introduce in this work is conceived to automatically elaborate the data generated by the biosensor in simultaneous measurements of multiple analytes (multiplex format). For this purpose, a first PCA is performed to rule out misbehaving channels and OPDs considering not only the confidence interval of the first principal components, but also the Q-residual and T2-Hotelling distances (i.e., the Q-residual analysis indicates how well each sample conforms to the model, while the T2-Hotelling distance is a measure of the variation in each sample within the PCA model). This analysis is performed in blocks: at first, the responses from all the channels with the same biofunctionalization are compared in presence of a specific analyte, expecting to observe a similar behavior; then, the responses from all the channels exposed to the same specific analyte but having different biofunctionalizations are also compared, this time assuming to observe significantly different behavior. Channels deviating from the above described behavior indicate aspecificity on the interaction of biomolecules. The lack of specificity could be explained by several reasons, as a cross-reactivity of the different analytes used on the multiplex sensor or cross-contamination within the different channels during the immobilization of the biomolecules. From this point onward, any channel or OPD deviating from the expected behavior due to aspecific interactions is defined as "abnormal," or as having "abnormal behavior," and excluded from the analysis. The developed algorithm can automatically identify the channels suitable for the detection of analytes on the multiplex sensor, and discard the abnormal ones which may lead to a misinterpretation of the results.

The data cleaning is then completed with a second analysis of residuals, used to remove outliers in measurements from the signals.[37] A last PCA is finally employed as a dimensionality reduction technique to smooth the sensorgrams, using only the first components to reconstruct the signal and thus removing the noise. The analytical result produced by the algorithm described above is in full agreement with the experimental quantification of the analyte, proving its functionality over several datasets, as well as demonstrating its ability to discriminate between biofunctionalized and reference channels. Moreover, this automated analysis provides a sound validation of the experimental methodology for data collection.

Figure 3a reports a representative self-testing measurement (sensorgram) due to Δn changes over the NPG sensing surface of the sensor, for all the working channels of the sensor, after signal reconstruction with the double PCA analysis. The signal from each channel is reported as response difference (%), that is the difference with respect to the baseline, divided by the baseline. It can be clearly observed the capability of the sensor of monitoring multiple events in real time (6 different reference solutions, each sample measured 6 times). The response difference averaged on all channels in response to the different sucrose concentrations (different Δn) are used to construct the calibration curve shown in Figure 3b. More details on data elaboration for the construction of the calibration curve are reported in the Supporting Information.

A linear increase of the signal as a function of Δn can be observed, with consistency of data within different channels. In this regard, the same calibration curve, with errors calculated as the standard deviation of the mean response averaged over channels, is reported in Figure S12 in the Supporting Information. To note, the linearity of the sensor response was verified also on a wider range of Δn (Figure S13, Supporting Information). A good correlation between the experimental and the linear fitting was still obtained ($R^2 > 0.99$), although the range of Δn investigated exceeds the expected range of Δn occurring in the quantitative calibrations of the assays. For the 1% sucrose injection corresponding to a Δn of about 10^{-3} RIU, a signal of 0.1% was obtained (considering raw data, a photocurrent variation of around 2 nA over a base current of around 2 µA, see Figure S10 in the Supporting Information). This is in accordance with the signal predicted from simulations (0.3%), as discussed above. From the calibration curve calculated from the self-testing procedure, the limit of detection (LOD) of the SPR biosensor prototype for bulk refractive index changes was extrapolated, reaching a value as low as $\approx 10^{-4}$ RIU.

New data analysis procedures were performed, aimed at further confirming the results above. In detail, several regression and classification models were trained to predict the response of the SPR biosensor prototype using the injected sucrose concentration as a target.[37–44] Among them, a recursive partitioning decision tree provided the best prediction of the sucrose concentration classes in terms of accuracy and specificity (Table S1 in the Supporting Information). From the confusion matrix (Table S2 in the Supporting Information) an overlap in test prediction between 0.1% of sucrose concentration and the baseline suggests that the LOD is reached at around 0.1% of sucrose concentration, corresponding to a bulk refractive index change of 10^{-4} RIU. This is in accordance with the experimental results

ADVANCED
SCIENCE NEWS
www.advancedsciencenews.com
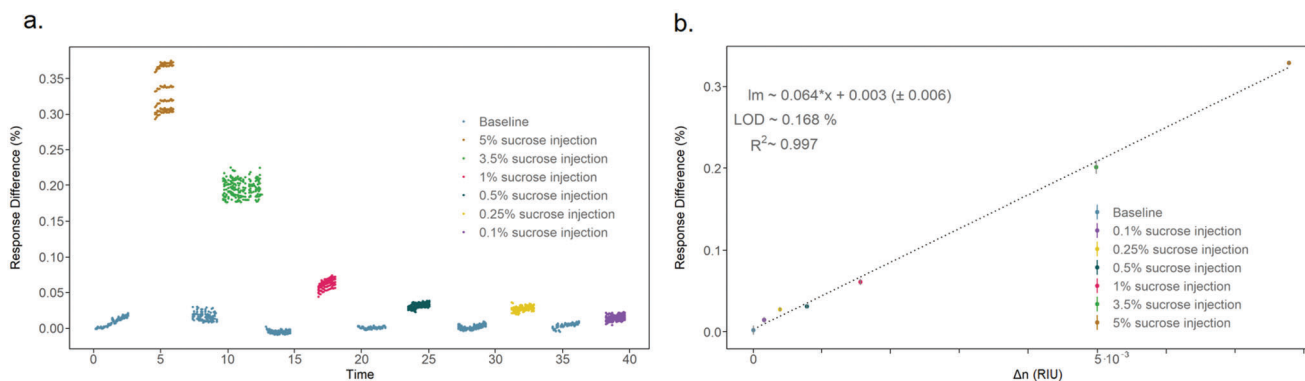
ADVANCED
MATERIALS
www.advmat.de

Figure 3. a) Sensorgram for sucrose solutions for different channels of the chip, after signal reconstruction through PCA analysis. All data are normalized with respect to the baseline before injection. b) Linearity plot of the signal of the sensor, normalized to the baseline, averaged over all the working channels, versus refractive index variations (Δn) during self-testing. The error associated to each plotted point is calculated as the average standard deviation of the mean values of the sensor signals for that sucrose concentration over all the working channels, while the LOD was calculated as 3.3 times the deviation of the signal divided by the slope of the calibration curve.

and gives consistency to the LOD calculated from the calibration curve.

Notably, an ad hoc experiment was carried out to compare the LOD of our SPR biosensor prototype with a reference benchtop SPR instrument, that being the Biacore 3000 (Figure S14a, Supporting Information). The experiment consisted in performing a calibration procedure with sucrose solutions and evaluating the LOD for both systems. In this direct comparison, the LOD of the SPR biosensor prototype resulted only one order of magnitude higher with respect to the benchtop SPR instrument, which is a highly developed instrument. Notably, the LOD of the SPR biosensor prototype here developed is still competitive with other SPR miniaturized sensors, which are nonetheless at an inferior level of integration.[45]

2.5. Biosensing of Analytical Targets and Calibration

According to the procedure described in the Experimental Section, the biorecognition elements were immobilized on the different channels of the optoplasmonic chip (Figure 1a) as follows: strep-BSA selective immobilization was provided on channels 2 and 5, channels 1 and 4 were functionalized with lactoferrin pAb, while channels 3 and 6 were only functionalized with bovine serum albumin (BSA) to be used as reference channels. Indeed, as in many other SPR techniques where specificity of detection is based on biomolecular recognition, the possible occurrence of false-positive signals due to aspecific interactions is taken into account by use of a reference channel. BSA is often used in SPR techniques to passivate the sensing surface of the reference channel to prevent reactivity toward any biological target under investigation.[46] To note, we used other blocking molecules (i.e., the blocking buffer described in Section 2.3 and in the Experimental Section) to further deactivate and minimize the number of surface nonspecific groups.

We highlight that the sequence of assays for streptomycin and lactoferrin is performed by injections in the meander microfluidic circuitry, thus on all the channels of the sensor chip (multiplex format), to proof its multiplex capability. As a consequence,

any possible cross-reactivity within analytes and channels has been carefully monitored and evaluated by the PCA analysis.

2.5.1. Streptomycin Assay

After the assembly of the SPR biosensor prototype (procedure reported in Figure S1 (Supporting Information), prototype shown in **Figure 4**a) and assessment of its functionality by self-testing with standard solutions (Section 2.4), the prototype functionality was tested for biosensing of the selected analytical targets.

The streptomycin assay was performed as a first qualitative analytical test of the SPR biosensor prototype. The strep-mAb was injected and data recorded for the interaction of the strep-mAb and the immobilized strep-BSA. For the competitive test, the streptomycin standard solution was prepared at a final concentration of 10 µg mL^{-1} and mixed with the streptomycin mAb.

After the streptomycin assay, the two different PCA approaches described for the self-testing were applied to the raw data. The PCA analysis of the raw data obtained by the injection of streptomycin mAb confirmed a specific response from channel 5 (functionalized with strep-BSA). This channel was successfully selected by the algorithm for the measurement of streptomycin analyte. The PCA analysis also confirmed the absence of a specific response to the streptomycin mAb injection in channel 3 (functionalized with BSA), thus channel 3 was successfully selected as reference channel by the algorithm. In addition, the PCA evidenced the occurrence of aspecific responses to streptomycin mAb from channels 1 and 4 (both functionalized with lactoferrin pAb), and from channel 6 (only functionalized with BSA). The aspecific response could be due to a variety of effects, i.e., contamination with strep-BSA during biofunctionalization. On the other hand, cross-reactivity of streptomycin mAb with Lactoferrin pAb or BSA must be excluded since it was not observed during assay development on the SPR benchmark instrument (data not shown). However, the presence in the optoplasmonic chip layout of two biofunctionalized channels for each assay, and two reference channels, reduces the failure rate of multiplex analysis after the exclusion of abnormal channels from the
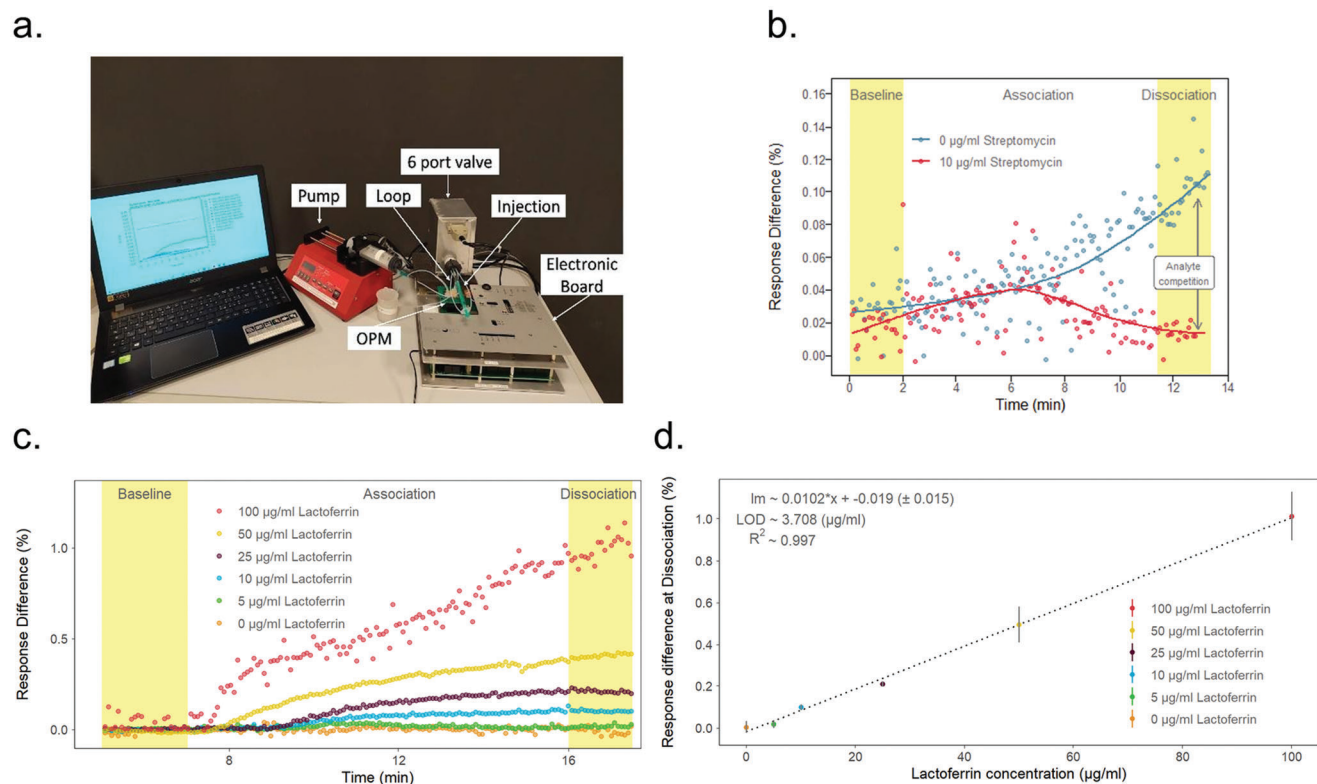
2208719 (7 of 13)

Figure 4. a) Picture of the complete sensor prototype: the optoplasmonic chip integrated into the electronic hardware and endowed with the meander microfluidic flow cell. The externally connected automatic syringe pump, injection valve and waste chamber are used for the fine control of flowing of the reagents during the measurements. b) Sensorgrams obtained during the streptomycin assays: competitive test in presence of 10 µg mL^{-1} of streptomycin (blue line) and competitive test in absence of streptomycin (red line). c) Sensorgrams obtained from several measurement cycles of lactoferrin solutions at varying concentrations (0, 5, 10, 25, 50, 100 µg mL^{-1}) in the direct assays. d) Dose–response curve of the sensor for the lactoferrin assays. The calculated LOD is 3.7 µg mL^{-1}.

PCA. The sensorgrams for the streptomycin assay obtained after data analysis are shown in Figure 4b and follow the expected kinetics (described in Figure S15 of the Supporting Information). In absence of streptomycin, it can be observed an increase of the signal after the injection of the streptomycin mAb only. This increase is stable during the dissociation phase, which demonstrates the correct antibody–antigen interaction (strep-BSA and streptomycin mAb). On the contrary, a signal drop is observed after injection of a sample containing both the streptomycin mAb and free streptomycin at a concentration of 10 µg mL^{-1}. This indicates inhibition of the binding of the streptomycin mAb to the strep-BSA and confirms the effectiveness of the designed (qualitative) competitive assay for streptomycin, at the given concentration.

2.5.2. Lactoferrin Assay

For demonstrating the possibility to use the proposed SPR biosensor prototype for the quantitative detection of a relevant milk quality target, a semi-quantitative assay for lactoferrin was performed. As described previously, the lactoferrin pAb was immobilized on channels 1 and 4 of the chip. After the acquisition of the baseline, a sequence of serially diluted lactoferrin samples were injected and response data recorded.

The same data elaboration and analysis as described for the streptomycin assay was used for the lactoferrin assay. The PCA analysis evidenced a specific response to Lactoferrin from channels 1 and 4 (functionalized with lactoferrin pAb). Within these two channels, channel 1 was selected by the algorithm as the sensing channel for the lactoferrin assay. The PCA analysis also excluded the occurrence of any specific response to Lactoferrin from channel 3 and 6 (only functionalized with BSA). Within these two channels, Channel 3 was selected by the algorithm as the reference channel (as for the streptomycin assay). To note, the PCA analysis also excluded cross-reactivity or aspecific response to lactoferrin from Channels 2 and 5 (functionalized with strep-BSA), at any of the selected concentrations tested. The sensorgrams acquired from channel 1 upon injection cycles of lactoferrin solutions at different concentrations are plotted in Figure 4c. Collecting the signal for only about 15 min (for each injection cycle), it is possible to follow the whole kinetics of biorecognition (Figure S15 in the Supporting Information).

The signal increases when compared to the baseline during the association phase. This indicates a specific recognition of the lactoferrin antigen by the immobilized lactoferrin pAb. Furthermore, the signal is constant during the dissociation phase when the surface is rinsed with a running buffer. This confirms that the lactoferrin proteins are effectively captured on the sensing surface by the lactoferrin pAb.

**ADVANCED
SCIENCE NEWS**

www.advancedsciencenews.com

**ADVANCED
MATERIALS**

www.advmat.de

The construction of the lactoferrin dose-response curve was done by considering the dissociation region. A linear increase of the signal over the baseline is observed for lactoferrin solutions with increasing concentrations (Figure 4d). This confirms that the chosen range of concentrations of the lactoferrin assays stays in the range of linear correlation between the analyte concentration and the number of antigen–antibody complexes formed on the sensing surface, with no saturation issues. From the dose–response curve, a LOD for lactoferrin as low as 3.7 μg mL^{-1} was calculated.

The presented output of the SPR biosensor prototype is very promising if compared to the performance of the benchtop SPR instrument (Biacore 3000) when the same direct immunoassay for lactoferrin was implemented. Indeed the LOD value extrapolated from the dose-response curve obtained by Biacore 3000 is higher (around 30 μg/ mL^{-1}, please consider Figure S14b, Supporting Information). However, we did not perform a systematic and throughout optimization of the measurement protocol in the benchmark assay, thus a lower LOD might be expected for the direct lactoferrin immunoassay.

Overall, the low LOD of the proposed SPR biosensor prototype will enable the detection of lactoferrin in real milk samples, when a proper sample preparation is defined and optimized accordingly. It is well-known that milk samples might be suitably diluted and filtered before analytical measures in order to limit possible adverse effects from the milk matrix. This experimental activity is out of the scope of the present work. However, the sensing dynamic range is sufficient for detecting lactoferrin at levels relevant to real samples.[47]

3. Conclusions

We report on the realization and demonstration of an innovative miniaturized optical biosensor for point-of-need analysis which is based on the unprecedented design and combination of the following elements: i) monolithically integrated organic light-emitting and light-sensing components (such as OLEDs and OPDs), and ii) a biofunctionalized nanoplasmonic grating working as transducing surface for SPR label-free detection. A stripe-like target-selective biofunctionalization of the transducing surface enables multiplexed detection in the sensor since multiple channels allocating miniaturized light-emitting/analyte-sensing/light-detecting units are present within a single optoplasmonic chip. In particular, we demonstrated the use of the sensor for the detection of a high-molecular-weight analyte (i.e., lactoferrin) by means of a direct assay, and of a low-molecular-weight analyte (i.e., streptomycin) by means of a competitive assay. In order to better assess the operability of the sensor prototype, a microfluidic module is integrated on top of the transducing surface to precisely control the volume of the solutions (standard, buffer, sample, regeneration) during the measurements and a stand-alone electronic hardware houses the optoelectronic chip for enabling analog amplification of the read-out electrical signal.

Self-testing and calibration of single channels by using sucrose solutions ensured result accuracy and repeatability, while data consistency was demonstrated through multivariate statistical principal-component analysis on wide datasets obtained from the collected sensorgrams. As a result, we demonstrated that the sensor can provide quantitative linear response when exposed to a refractive index change of the surrounding bulk medium, reaching a LOD of 10^{-4} RIU, that is only one order of magnitude lower than the LOD of the reference benchtop SPR instrument from Biacore.

When detecting the two target analytes in buffer solutions at concentrations relevant for milk quality and safety (i.e., tens of μg mL^{-1} for lactoferrin, and 10 μg mL^{-1} for streptomycin), a LOD as low as 3.7 μg mL^{-1} was extrapolated from the curve, which is in line with what obtained from the reference benchtop SPR instrument in the same experimental conditions.

The capability of multiplexing different analytes in a single quantitative measurement, tailoring sensing chips to specific locations and applications, with lab-technique accuracy providing quantitative results, means the proposed SPR biosensor prototype outperforms widely used immunoassays like enzyme-linked immunosorbent assay (ELISA) and lateral flow immunoassay (LFIA). Since ELISA is not portable on-site, a comparison the LFIA is more realistic. LFIAs are generally low cost and easy to use, but are single use and often only qualitative. We also highlight that the implemented automatized data processing method dramatically improves the quality of the presented data, and potentially allows the use of the sensor by nonexperts. In this way, nonskilled operators could use the sensor in a wide variety of scenarios, where real-time analytical results can make a significant difference allowing actions to be taken immediately.

Considering the previously mentioned ELISA, the here-presented SPR biosensor prototype has a competitive analytical performance, but will have distinct advantages in terms of cost per test, speed of analysis (i.e., 15 min-long measurement protocol) and multiplex capabilities. We highlight that the possibility to regenerate and thus reuse the sensing surface of the optoplasmonic chip up to 450 times, which is an inherent characteristics of NPG technology,[48] will highly reduce the cost per test, as in contrast to an ELISA. Finally, the implementation of an user-independent and reliable post-measure data analysis remarkably validates the use of the SPR biosensor prototype for real-setting application by nontrained users.

Overall, this work demonstrates that by an accurate design and integration of organic optoelectronics, nanoplasmonics, and advanced surface functionalization, reliable and performing PON analytical systems can be developed for real-setting applications, such food safety and quality. Furthermore, it is reasonable that such technologies would soon expand also toward IC and computing application fields, replacing current electronic-based technologies in many scenarios. The research and development in each of those technological fields will lead synergistically to a virtuous loop, allowing the production costs to be reduced and allowing their full potential to be soon exploited.[49]

4. Experimental Section

Fabrication of Monolithically Integrated Optical Transduction Elements (OLEDs and OPDs): Hole Transport Material (HTM) was supplied by Merck KGaA. Novaled Dopand p-side (NDP-9), Electron Blocking Material (EBM) and Electron Transport Material (ETM) were supplied by Novaled GmbH. Tris(8-hydroxy-quinolinate)aluminium (Alq3), Pt^{II}-tetraphenyltetrabenzoporphyrin (Pt(tpbp)), 9,9-bis[4-(*N*,*N*-bis-biphenyl-4-yl-amino)phenyl]-9H-fluorene (BPAPF), and 4,7-diphenyl-1,10-phenanthroline (BPhen) were purchased from Luminescence Technology

Corp. Zinc phthalocyanine (ZnPc) and fullerene-C60 were purchased from CreaPhys (Dresden, Germany). Fabrication was carried out on 200 mm square and 0.7 mm thick glass plates. First, the glass was cleaned by an ultrasonic bath in surfactants, rinsed with deionized water, dried in a Spin-Rinse-Dryer 2300S (Semitool), and heated under vacuum for 1 h at 120 °C. Then, glass plate was exposed to an oxygen/argon plasma, and the front side was coated with the OLED and OPD stack via thermal evaporation through fine metal masks at a pressure less than 2×10^{-4} Pa (Sunicel PLUS 200, Sunic Systems, Korea). The OLED and OPD deposition sequence follows the ones reported in Figure S16 (Supporting Information). Layer thicknesses of the OPD stack were optimized for maximum sensitivity at 770 nm. OLED/OPD structures were encapsulated using NPG coated cavity glass and epoxy glue and separated into individual samples via a scribe and break process (MDI Advanced Processing).

Characterization of OLEDs and OPDs: The OLED was tested in a glovebox, by using a standard SUSS probe station coupled to a B1500A Agilent semiconductor device analyzer as the current source/electrical readout, and by measuring the optical power output from the top side by using a calibrated silicon photodiode with responsivity = 0.49 A W^{-1} at 766 nm. Electroluminescence spectra on the encapsulated OLEDs were collected by a calibrated optical multichannel analyzer PMA-11 from Hamamatsu. OLED radiance at measurement continuous working (Figure S17a, Supporting Information) was carried out using the DMS 401 system by Autronic-Melchers.

External quantum efficiency (EQE) was measured by using a homemade setup including an ASBN-W100 tungsten–halogen light source coupled with a Digikröm CM110 1/8m monochromator (Spectral Products), a Chopper MC2000 (THORLABS Inc.), a lock-in amplifier 7270 (AMETEK Inc.), and a current preamplifier 5182 (AMETEK Inc.). A Standard Photodiode Power Sensor S120VC (THORLABS Inc.) was used as the reference. EQE measurements were performed with the OPD at zero bias and at a chopper frequency of 83 Hz. The operational stability of the OPD photocurrent driven at 0 V was monitored over 30 min under continuous illumination from the top side with an inorganic LED from THORLABS, with 30 μW of optical power and an emission centered at 770 nm. Photocurrent was collected with an Electrochemical Workstation (Autolab, PGSTAT128N+ECD module). Before the measurement, the LED was switched on and warmed up for 10 minutes. Results are shown in Figure S17b in the Supporting Information.

The OLED and OPD should exhibit stable operation at least for the time required for the analytical measurement (around 15 minutes), under ambient conditions. The photocurrent stability of the OPD was then verified in the complete optoplasmonic chip (Figure S18 in the Supporting Information).

Fabrication and Chemical Functionalization of the NPG: The fabrication and characterization have been reported in the previous work.[22] Briefly, the system is constituted of a hexagonal lattice of polymeric pillars embedded in a relatively thick gold layer (about 150 nm, please consider Figure S6 in the Supporting Information), prepared through colloidal lithography and plasma etching techniques. In details, the plasmonic grating was fabricated by using a monolayer of hexagonally ordered polystyrene beads (diameter = 500 nm) as a sacrificial mask for the etching of a 150 nm thick poly(methyl methacrylate) (PMMA) layer, followed by gold deposition (nominal 150 nm) and mask removal. The resulting surface supports the interaction of the propagating SPR modes, typical of the usual SPR detection, with the localized ones correlated to the polymeric pillars, allowing the direct detection of the refractive index sensitive plasmonic features by a reflectance measurement from the back (substrate) side, avoiding the use of an optical prism.[23–24]

For NPG functionalization, a commercial kit was acquired from Lucidant Polymers, containing the MCP-2F polymer and buffer solutions. The MCP-2F polymer has a chemical structure comprising the monomers *N,N*-dimethylacrylamide (DMAM), 3-(methacryloyl-oxy)propyltrimethoxysilane (MAP), *N,N*-acryloyloxysuccinimide (NAS) and monomers of perfluorinated carboxylic acids (PFCAs) bearing fluorine moieties. The MCP-2F stock was diluted 1:50 in coating buffer and the sensor surface was incubated with this solution for 30 min at room temperature. Next, the sur-

face was rinsed with water and dried under nitrogen flow. Contact angle and optical characterization were carried out in the NPG before and after the functionalization. Reflectance measurements were applied for optical characterization of the chip surfaces. The measurements were performed with an inverted microscope (Axiovert 25, Zeiss) coupled with a compact USB fiber optic spectrometer (USB4000, OceanOptics). A halogen lamp was used as the light source, and the spectra were acquired over the range from 400 to 1000 nm. Light was directed to the surface (from the glass substrate side) through a 5× objective with a NA = 0.13 (Epiplan 5x, Zeiss), and the back-reflected light was collected by the same objective lens. Reflectance spectra measured close to normal before and after NPG functionalization are shown in Figure S19 in the Supporting Information.

Optical Simulations: The 3D simulation model developed ad hoc in the previous work was adapted to the new optoelectronic performances, geometrical and structural characteristics of the individual components in the optoplasmonic chip.[22] Briefly, the simulation model includes two parts: i) the optical simulation of the NPG as a "programmable mirror" component, including angular spectral reflection efficiencies interpolated from discrete experimental data, for different media at the surface of the NPG; this was performed by means of the Fourier model method (FMM, also called rigorous coupled-wave analysis or RCWA); ii) the optical simulation of the complete optoplasmonic system based on a field tracing approach, considering diffraction, interference (phase), and polarization. The entire 3D optical simulation of the optoplasmonic chip was implemented by using software Virtuallab Fusion (latest version 2021.1, build 1.180).

Biofunctionalization of the Optoplasmonic Chip: For the immobilization of receptor biomolecules on the surface of the NPG, a microfluidic device was designed to match the layout of the channels of the sensor (Figure S20, Supporting Information). The microfluidic device consists of seven microchannels, with dimensions and spacing of the channels (1.54 mm width, 0.13 mm height, 2.9 μL volume each) defined by the OLEDs of the optoplasmonic chip. The microfluidic channels are connected to an external peristaltic pump, to provide a different protein sample on each one of the seven channels of the optoplasmonic chip, ensuring multiplex analysis with the same chip. The microfluidic device consists also of a holder plate for the optoplasmonic chip with alignment pins, which ensure reproducible alignment between the optoplasmonic chip and the microfluidic device. The microfluidic device is attached to the optoplasmonic chip by a laser-cut sealing foil.

The protein samples were diluted in the buffer for immobilization (Spotting buffer from Lucidant polymers) to 150 μg mL^{-1}, and they were introduced to the chip channels by a circular flow of 10 μL min^{-1}, overnight at room temperature. Following the immobilization of the proteins, the microfluidic device was removed, the whole chip was washed with water to remove unbound proteins, and then incubated in the blocking buffer from Lucidant kit to passivate the remaining parts of the chip that were not biofunctionalized. As a last step, the chip was rinsed with water and dried, and assembled with the microfluidic meandering cell for the self-testing procedure and for the analytical measurements (see Figure S1 in the Supporting Information where a graphical sketch of the procedure of fabrication and assembly of the optoplasmonic chip is reported).

Microfluidic Flow Cell: For the analyte measurements, a meander microfluidic flow cell was fabricated by xurography and attached on the optoplasmonic chip surface (Figure S21 in the Supporting Information) that consists in the use of structured double-sided adhesive tapes (thickness 140 μm) and a structured polycarbonate sheet (thickness 250 μm).

The meandering flow cell had identical channel dimensions as used for prior immobilization of receptors resulting in a total flow chamber volume of 27 μL. The possible misalignment between the biofunctionalized channels of the optoplasmonic chip and microfluidic channels was minimized by settling alignment features used for the integration of the components. The resulting alignment error was <100 μm.

Electronic Hardware: The in-house designed and assembled electronic hardware allows to measure during the same analytical session all the 7 channels of the chip. The multiplex functioning of the chip is schematized in Figure S22 (Supporting Information). The electronic hardware includes the following components/functionalities: 1) low noise, high

**ADVANCED
SCIENCE NEWS**

www.advancedsciencenews.com

**ADVANCED
MATERIALS**

www.advmat.de

power supply rejection ratio (PSRR) power supplies; 2) a connector for the optical biosensor; 3) a connector to an external controller (computer); 4) low noise, high stability voltage references; 5) oscillators; 6) low-noise, high-stability current source; 7) current modulator; 8) a multiplexer for the OLEDs; 9) OPD amplifiers; 10) OPDs multiplexer; 11) filters; 12) demodulators; 13) temperature sensors front-end.

As the photocurrent of the OPDs is very low, each OPD has its own amplifier (to optimize circuitry layout against leakage current). These amplifiers configured as "transimpedance amplifiers" directly convert the current signal into voltages to simplify the rest of the acquisition chain.

The analog amplication consists in the following steps: 1) conversion of OPD photocurrent to voltage using a trans-impedance amplifier (gain: $1\,V\,\mu A^{-1}$), 2) boosting the trans-impedance amplifier output voltage (gain: 1), 3) analog-to-digital conversion using a 16-bit ADC (with resolution: $\approx 19\,pA$ per Least-Significant-Bit).The performance and the electrical noise of the fully assembled electronic hardware was tested through laboratory instruments. The electronic hardware showed a total noise of 11.9 pA and a photocurrent resolution of 38.14 pA, over an OPD base photocurrent of 2.5 µA (please consider Figure S10 in the Supporting Information where raw dataset of collected photocurrent from OPD is reported). In addition, an accuracy of 50 pA steps on a 500 pA scale was also demonstrated.

Development of Immunoassays for SPR Measurements: Immunoassays were developed and tested in the benchtop SPR instrument Biacore 3000. The lactoferrin polyclonal antibody (pAb) was purchased from Bethyl laboratories (Montgomery, USA) while the streptomycin monoclonal antibody (mAb) was purchased from Unibiotest (Wuhan, China). A conjugate of streptomycin coupled to BSA as a carrier protein, was prepared in-house (strep-BSA).

Immobilization of the lactoferrin pAb and the strep-BSA conjugate onto the biosensor CM5 chip surface was performed in the Biacore 3000 using the buffer scouting module for optimal coupling efficiencies. The CM5 chip was activated by the standard EDC/NHS Biacore method. The Lactoferrin assay was designed as a direct assay. To create this direct assay, the lactoferrin pAb was diluted to a concentration of 50 µg mL^{-1}, in the optimal acetate buffer pH 4.5, and injected several times into the activated channel on the CM5 chip, aiming for a total of 10^4 response units (RU). The reference measurement channel was activated and then deactivated by injecting ethanolamine. Next, lactoferrin standards, ranging from 0 to 500 µg mL^{-1}, were injected, 100 µL of each standard at 100 µL min^{-1}. Between each injection, the chip was regenerated by a 40 µL injection of 10×10^{-3} M HCl at 100 µL min^{-1}. By plotting the maximum responses of the different lactoferrin standards, a dose–response curve was constructed. For the streptomycin assay, the strep-BSA conjugate was diluted to 80 µg mL^{-1} for immobilization on the CM5 chip surface, in acetate buffer pH 4.5, using the same amine coupling procedure as for the lactoferrin pAb aiming for a total of 10^4 RU. The activated reference channel was coupled with BSA under the same circumstances. Next, standard solutions of streptomycin in HBS-EP (composition: 0.01 M HEPES pH 7.4, 0.15 M NaCl, 3×10^{-3} M EDTA, and 0.005% surfactant P20) were prepared (1000–0.01 ng mL^{-1}). The streptomycin mAb was diluted to a final concentration of 5 µg mL^{-1} and mixed 1:1 with each streptomycin standard. From each standard-mAb mixture, 50 µL was injected at a flow of 20 µL min^{-1}. Between each injection, the chip was regenerated with a 5 µL injection of 50×10^{-3} M HCl at 20 µL min^{-1}. Using the maximum responses of the different streptomycin standards, a dose–response curve could be constructed. Additionally, 10-fold serial dilutions (1000 to 0.1 ng mL^{-1}) of all the aminoglycosides available in our laboratories (di-hydrostreptomycin, apramycin, gentamycin, tobramycin, neomycin, paromomycin, spectinomycin, and kanamycin A) were prepared and tested for their cross-reactivity in the streptomycin assay.

Protocol of Measurement—Self-Testing: After having filled the meander microfluidic cell with ultrapure water, the self-testing measurement started and data are collected through the electronic hardware. Measurement cycles were performed at a flow rate of 10 µL min^{-1}. First, a solution of sucrose in ultrapure water was injected to replace the liquid filling the cell. This sucrose solution remained in the flow cell for a few minutes to allow for stabilization of the optoelectronic components and signal acquisition. Next, a water sample was injected. The cycles of injection-stabilization

were repeated for different sucrose concentrations (5%, 3.5%, 1%, 0.5%, 0.25%, 0.1% in water) to complete the self-testing session. Calculation of the response difference (%) and of the correction factors for each channel and OPD of the sensor, are reported in the Supporting Information, in the section *Processing of Datasets* reported below Figure S11 in the Supporting Information.

Protocol of Measurement—Tests of Assays on the Sensor: The in-house fabricated microfluidic flow cell (Figure S21, Supporting Information), attached to the optoplasmonic chip and connected to the electronic hardware, was connected to an external syringe pump (NE1000 from syringepump.com USA) and a six-port injection valve (TitanEx MLP777-601 from Idex Health&Science USA) for the control of fluidics during the immunoassays. HBS-P (composition: 0.01 M HEPES pH 7.4, 0.15 M NaCl and 0.005% surfactant P20) was used as a running buffer. The measurement cycles were performed at a flow rate of 10 µL min^{-1}. Each measuring cycle involved recording the baseline signal during 2 min with running buffer, during 10 min after injection of the sample (association phase), during 2 min of washing off the unbound sample with running buffer (dissociation phase), and during 30 s of regeneration. The regeneration phase (injection with 10×10^{-3} M HCl) was performed on all the channels of the chip, to remove the bound proteins and regenerate the sensing surface for the next measurement. Lactoferrin (molecular weight: 80 kDa) and streptomycin (molecular weight: 582 Da) were the analytical targets. The sensor channels which contained the immobilized lactoferrin pAb (channels 1 and 4) were used for the lactoferrin assay. Solutions of lactoferrin spiked in running buffer, at a concentration of 0, 5, 10, 25, 50, and 100 µg mL^{-1}, were tested. The streptomycin assay was designed as an inhibition assay. The sensor channels with immobilized strep-BSA (channels 2 and 5) were used to interact with the streptomycin mAb. Therefore the streptomycin mAb was diluted to 38 µg mL^{-1} in running buffer. Samples containing the competitor streptomycin at 0 and 10 µg mL^{-1} were mixed 1:1 with the streptomycin mAb solution. In both assays (lactoferrin and streptomycin), the BSA immobilized channels (3 and 6) were used as reference. The response obtained from the analyte-selective channels was normalized to the reference channels to correct any nonspecific interaction and corrected by a channel-specific correction factor extrapolated from the self-testing procedure (see the Data Analysis procedure described in the Supporting Information in the section on processing of datasets reported below Figure S11 in the Supporting Information). The calibration curve and quantitative response from the sensor was extrapolated from the sensorgrams following the data analysis procedure described in the following section. The LOD for the lactoferrin detection was calculated as 3.3 times the deviation of response divided by the slope of the calibration curve.[50–52]

Statistical Data Analysis: The analysis of the collected datasets was performed in the *R* environment (*R* software environment used to run codes written in the *R* language), for statistical calculation and visualization. Datasets acquired during the self-testing measurements and during the assays were analyzed. The analysis was divided into several phases, some common to all the experiments, others specific to the desired target. Please consider Figure S11 in the Supporting Information for a graphical representation of the different processing of the collected datasets.

The common preprocessing phase consists of a data preparation step (e.g., formatting the channel names, converting the amplitude data into numeric and timestamp into date-time, removing null variance columns, if any, ...) and as a sensorgram preparation step, consisting of baseline subtraction and normalization to the baseline. The correct individuation of the region of data for the baseline selection was identified as a crucial step. To this end, a custom algorithm has been developed for identifying the areas of greatest stability before injections or, when this information was provided, within a range established a priori based on the measurement times. The baseline subtraction is thus performed, ensuring to spot and remove possible biases or artifact trends in the sensorgrams. Finally, each sensorgram is normalized with respect to its baseline (as described in the Supporting Information). After the common preprocessing phase, the data analysis by the PCA is carried out differently for the different test targets. Once the final dataset were obtained, it was necessary to identify the regions of interest for the analysis in all the measurement sessions, in particular the regions of response to the injection of the target and the

regions of dissociation (Figure S15 in the Supporting Information). For this purpose, an algorithm was written which, upon receipt of an indication of the time ranges where to search for events, identifies the areas of maximum stability and maximum slope and the elbow points that define them. In this way it is possible to associate a target variable that marks the significant events for the tests and that will then be used to obtain the final output, whether it is the calibration curve, the dissociation coefficient or the prediction of a classification model. Data in the calibration curves are reported as mean $\pm$ standard deviation.

Supporting Information

Supporting Information is available from the Wiley Online Library or from the author.

Conflict of Interest

The authors declare no conflict of interest.

Data Availability Statement

The data that support the findings of this study are available from the corresponding author upon reasonable request.

[1] L. Rodriguez-Saona, D. P. Aykas, K. R. Borba, A. Urtubia, *Curr. Opin. Food Sci.* **2020**, *31*, 136.

[2] F. di Nardo, M. Chiarello, S. Cavalera, C. Baggiani, L. Anfossi, *Sensors* **2021**, *21*, 5185.

[3] L. Zhang, C. Gu, H. Ma, L. Zhu, J. Wen, H. Xu, H. Liu, L. Li, *Anal. Bioanal. Chem.* **2019**, *411*, 21.

[4] D. Liu, J. Wang, L. Wu, Y. Huang, Y. Zhang, M. Zhu, Y. Wang, Z. Zhu, C. Yang, *Trends Anal. Chem.* **2020**, *122*, 115701.

[5] *Micro- and Nanotechnology Enabled Applications for Portable Miniaturized Analytical Systems* (Eds: S. Thomas, M. Ahmadi, T. A. Nguyen, A. Afkhami, T. Madrakian), Elsevier, Amsterdam, The Netherlands **2021**.

[6] M. Prosa, M. Bolognesi, L. Fornasari, G. Grasso, L. Lopez-Sanchez, F. Marabelli, S. Toffanin, *Nanomaterials* **2020**, *10*, 480.

[7] M. Kim, N. Park, H. J. Lee, J. Rho, *Nanophotonics* **2022**, *11*, 2389.

[8] P. N. Nge, C. I. Rogers, A. T. Woolley, *Chem. Rev.* **2013**, *113*, 2550.

[9] M. B. Kulkarni, N. H. Ayachit, T. M. Aminabhavi, *Biosensors* **2022**, *12*, 543.

[10] A. Minopoli, A. Acunzo, B. della Ventura, R. Velotta, *Adv. Mater. Interfaces* **2022**, *9*, 2101133.

[11] Y. Chen, J. Liu, Z. Yang, J. S. Wilkinson, X. Zhou, *Biosens. Bioelectron.* **2019**, *144*, 111693.

[12] Y. Liu, X. Zhang, *Micromachines* **2021**, *12*, 826.

[13] F. Yesilkoy, *Sensors* **2019**, *19*, 4287.

[14] P. Kozma, F. Kehl, E. Ehrentreich-Förster, C. Stamm, F. F. Bier, *Biosens. Bioelectron.* **2014**, *58*, 287.

[15] R. De, L. Rue, H. P. Herzig, M. Gerken, *Biomedical Optical Sensors*, Springer, Cham, Switzerland **2020**.

[16] C. Fuentes-Hernandez, W.-F. Chou, T. M. Khan, L. Diniz, J. Lukens, F. A. Larrain, V. A. Rodriguez-Toro, B. Kippelen, *Science* **2020**, *370*, 698.

[17] F. Li, A. J. Gillett, Q. Gu, J. Ding, Z. Chen, T. J. H. Hele, W. K. Myers, R. H. Friend, E. W. Evans, *Nat. Commun.* **2022**, *13*, 2744.

[18] R. Capelli, S. Toffanin, G. Generali, H. Usta, A. Facchetti, M. Muccini, *Nat. Mater.* **2010**, *9*, 496.

[19] D. Gedefaw, M. Prosa, M. Bolognesi, M. Seri, M. R. Andersson, *Adv. Energy Mater.* **2017**, *7*, 1700575.

[20] N. Gasparini, L. Lucera, M. Salvador, M. Prosa, G. D. Spyropoulos, P. Kubis, H. J. Egelhaaf, C. J. Brabec, T. Ameri, *Energy Environ. Sci.* **2017**, *10*, 885.

[21] M. Prosa, E. Benvenuti, M. Pasini, U. Giovanella, M. Bolognesi, L. Meazza, F. Galeotti, M. Muccini, S. Toffanin, *ACS Appl. Mater. Interfaces* **2018**, *10*, 25580.

[22] M. Prosa, E. Benvenuti, D. Kallweit, P. Pellacani, M. Toerker, M. Bolognesi, L. Lopez-Sanchez, V. Ragona, F. Marabelli, S. Toffanin, *Adv. Funct. Mater.* **2021**, *31*, 2104927.

[23] S. Giudicatti, F. Marabelli, P. Pellacani, *Plasmonics* **2013**, *8*, 975.

[24] B. Bottazzi, L. Fornasari, A. Frangolho, S. Giudicatti, A. Mantovani, F. Marabelli, G. Marchesini, P. Pellacani, R. Therisod, A. Valsesia, *J. Biomed. Opt.* **2014**, *19*, 017006.

[25] I. Vikholm-Lundin, W. M. Albers, *Biosens. Bioelectron.* **2006**, *21*, 1141.

[26] H. Huang, C. He, Y. Zeng, X. Xia, X. Yu, P. Yi, Z. Chen, *Biosens. Bioelectron.* **2009**, *24*, 2255.

[27] J. W. Waswa, C. Debroy, J. Irudayaraj, *J. Food Process. Eng.* **2006**, *29*, 373.

[28] D. B. Kell, E. L. Heyden, E. Pretorius, *Front. Immunol.* **2020**, *11*, 1221.

[29] K. Shimazaki, K. Kawai, *Biochem. Cell Biol.* **2017**, *95*, 69.

[30] R. Wang, J. Wang, H. Liu, Y. Gao, Q. Zhao, S. Ling, S. Wang, *Food Chem.* **2021**, *338*, 127820.

[31] L. Liu, D. Kong, C. Xing, X. Zhang, H. Kuang, C. Xu, *Anal. Methods* **2014**, *6*, 4742.

[32] L. A. Brunton, D. Duncan, N. G. Coldham, L. C. Snow, J. R. Jones, *Vet. Rec.* **2012**, *171*, 296.

[33] E. Peterson, P. Kaur, *Front. Microbiol.* **2018**, *9*, 2928.

[34] W. Haasnoot, E. E. M. G. Loomans, G. Cazemier, R. Dietrich, R. Verheijen, A. A. Bergwerff, R. W. Stephany, *Food Agric. Immunol.* **2002**, *14*, 15.

[35] C. Zilio, L. Sola, F. Damin, L. Faggioni, M. Chiari, *Biomed. Microdevices* **2014**, *16*, 107.

[36] H. Abdi, L. J. Williams, *Wiley Interdiscip. Rev. Comput. Stat.* **2010**, *2*, 433.

[37] L. E. Mujica, J. Rodellar, A. Fernández, A. Güemes, *Struct. Health Monit.* **2011**, *10*, 539.

[38] L. Breiman, *Int. J. Mach. Learn. Cybern.* **2001**, *45*, 5.

[39] M. Jahn, Artificial Neural Network Regression Models: Predicting GDP Growth, https://www.econstor.eu/handle/10419/182108 (accessed: September **2022**).

[40] A. Karatzoglou, D. Meyer, W. Wien, K. Hornik, *J. Stat. Software* **2006**, *15*, 1.

[41] K. Khadiev, I. Mannapov, L. Safina, arXiv:1907.06840, **2019**.

[42] M. Kuhn, *J. Stat. Software* **2008**, *28*, 1.

[43] J. Schmidhuber, *Neural Networks* **2015**, *61*, 85.

[44] Z. Zhang, *Ann. Transl. Med.* **2016**, *4*, 1.

[45] A. L. Moras, V. Silva, M. C. M. M. Souza, G. A. Cirino, A. A. G. von Zuben, L. A. M. Barea, N. C. Frateschi, *IEEE Photonics J.* **2020**, *12*, 6802910.

[46] C. M. Miyazaki, F. M. Shimizu, M. Ferreira, in *Micro and Nano Technologies, Nanocharacterization Techniques* (Eds: A. L. Da Róz, M. Ferreira, F. de Lima Leite, O. N. Oliveira), William Andrew Publishing, Norwich, NY, USA **2017**, Ch. 6.

[47] A. Mortari, L. Lorenzelli, *Biosens. Bioelectron.* **2014**, *60*, 8.

[48] S. Joshi, R. M. Annida, H. Zuilhof, T. A. van Beek, M. W. F. Nielen, *J. Agric. Food Chem.* **2016**, *64*, 8263.

[49] J. García-Rupérez, *Expert Rev. Mol. Diagn.* **2021**, *21*, 995.

[50] T. Wenzl, J. Haedrich, A. Schaechtele, P. Robouch, J. Stroka, *Guidance Document on the Estimation of LOD and LOQ for Measurements in the Field of Contaminants in Feed and Food; EUR 28099, Publications Office of the European Union*, Luxembourg **2016**, https://doi.org/10.2787/8931.

[51] E. Desimoni, B. Brunetti, *Pharm. Anal. Acta* **2015**, *6*, 355.

[52] A. Shrivastava, V. B. Gupta, *Chron. Young Sci.* **2011**, *2*, 21.